Journal of Materials Chemistry A

PAPER

View Article Online
View Journal | View Issue

Cite this: J. Mater. Chem. A, 2018, 6, 23712

Stabilization of all-solid-state Li–S batteries with a polymer–ceramic sandwich electrolyte by atomic layer deposition†

Jianneng Liang,[a] Qian Sun,[a] Yang Zhao,[a] Yipeng Sun,[a] Changhong Wang,[a] Weihan Li,[a] Minsi Li,[b] Dawei Wang,[a] Xia Li,[a] Yulong Liu,[a] Keegan Adair,[a] Ruying Li,[a] Li Zhang,[c] Rong Yang,[c] Shigang Lu,[c] Huan Huang[d] and Xueliang Sun *[a]

Received 17th September 2018
Accepted 27th October 2018

DOI: 10.1039/c8ta09069f

rsc.li/materials-a

All-solid-state lithium–sulfur batteries (ASSLSBs) are promising candidates as the power source for future electric vehicles due to their high energy density and superior safety properties. However, one of the major challenges of state-of-the-art ASSLSBs is related to the high interfacial resistance resulting from the instability between the solid-state electrolyte (SSE) and electrodes and/or the side reactions between polysulfides and SSE. Herein, we propose and demonstrate the significant enhancement of the cycling stability of an ASSLSB through atomic layer deposition interfacial engineering on the polymer/oxide ceramic/polymer sandwich-structured SSE. The results show that as few as 10 cycles of ALD Al_2O_3 on the LATP can endow ASSLSBs with a discharge capacity of 823 mA h g^{-1} after 100 charge/discharge cycles, which is almost two times higher than that of the ASSLSB without an ALD coating and that of a Li–S battery with a liquid-based electrolyte. Such improvement is attributed not only to the blocking of the polysulfide shuttling effect *via* the use of a sandwich SSE but also the significant reduction of the side reaction between the polysulfide and oxide ceramic SSE, which introduces high interfacial resistance and degrades the electrochemical performance. The protection role and mechanism of the ALD layer is also confirmed and revealed by XRD, SEM and XPS measurements.

Introduction

Lithium–sulfur (Li–S) batteries are promising candidates for application in portable electronics and electric vehicles (EVs), and have received significant attention due to the natural abundance, low cost and environmental friendliness of sulfur. In addition, sulfur possesses high theoretical specific capacities and energy densities which are up to 1675 A h kg^{-1} and 2500 W h kg^{-1},[1,2] respectively, *i.e.* a 6-fold increase in specific energy density over that of the $LiCoO_2$ cathode in conventional LIBs.[3] However, several critical obstacles have hindered conventional Li–S batteries using liquid electrolyte from achieving practical application. One of the major challenges is that polysulfide intermediates are soluble in liquid electrolyte, resulting in the polysulfide shuttle effect[4,5] which induces rapid capacity fading during cycling and results in low coulombic efficiency.[1,6,7] Meanwhile, a liquid-based electrolyte contains flammable and volatile solvents, leading to serious safety concerns. Accordingly, the development of all-solid-state Li–S batteries (ASSLSBs) is regarded as a potential strategy to solve these problems in Li–S batteries.[7,8] The application of a non-flammable solid-state electrolyte (SSE) is expected to eliminate the possibilities of polysulfide shuttling to realize safe and long-life ASSLSBs as a desirable candidate for application in future EVs.

Various choices of SSEs for ASSLSBs have previously been reported, such as poly(ethylene oxide) (PEO) based solid polymer electrolytes (SPEs),[9,10] oxide-based SSEs,[11] sulfide-based SSEs[12–14] and sandwich-type hybrid electrolytes.[15] In particular, the application of sandwich-type hybrid electrolytes in ASSLSBs has received significant attention due to their high ionic conductivity, ability to prevent lithium dendrite formation and good electrode wetting properties. All of the above-mentioned merits can contribute to improved cycling performance.[16–18]

However, the development of ASSLSBs based on all-solid-state hybrid SSEs has been hindered due to several challenges, including: (i) low ionic conductivity at room temperature; (ii) instability between the SSE and electrode materials; (iii) high interfacial resistance. The instability between the SSE and electrodes comes from the side reactions between the SSE and electrode materials, resulting in degradation of the SSE and

[a]Department of Mechanical and Materials Engineering, University of Western Ontario, London, ON N6A 5B9, Canada. E-mail: xsun@eng.uwo.ca

[b]Department of Chemistry, University of Western Ontario, London, ON N6A 5B7, Canada

[c]China Automotive Battery Research Institute Co., Ltd., 5th Floor, No. 43, Mining Building, North Sanhuan Middle Road, Haidian District, Beijing 100088, China

[d]Glabat Solid-State Battery Inc., 700 Collip Circle, Suite 211, London, ON N6G 4X8, Canada

† Electronic supplementary information (ESI) available. See DOI: 10.1039/c8ta09069f

thus lowered ionic conductivity. For example, the reduction of Ti-containing SSEs such as NASICON-type $Li_{3-2x}(Al_{1-x}Ti_x)_2(PO_4)_3$ (LATP) and perovskite-type $Li_{3x}La_{2/3-x}TiO_3$ (LLTO) is observed when placed in contact with a lithium anode[16,19] or other reductant species such as polysulfides.[20] LATP is one of the most studied oxide-based SSEs that has already been used in quasi-solid-state Li–S batteries.[20,21] However, there is a critical problem that needs to be addressed when using LATP in Li–S batteries, which is the instability of LATP against polysulfide species. Manthiram's group used SEM, XRD and XPS to study the reduction of LATP by polysulfides and the results indicate that polysulfides can deteriorate the performance of the LATP SSE, which results in degradation of Li–S battery performance.[20]

Therefore, the protection of LATP from reduction by polysulfides is critical to build long-life ASSLSBs. The properties of the protection layer should meet two primary requirements: (i) chemical stability in a reducing environment and (ii) enabling diffusion of Li^+ ions through the protection layer. As a promising protection technique, atomic layer deposition (ALD) is a unique technology that can realize conformal thin film deposition with excellent coverage and controllable deposition thickness at the nanoscale due to the use of self-limiting reactions.[22–24] More importantly, the deposition temperature of ALD can be low enough to avoid side reactions between the deposited material and the substrate. Accordingly, it is expected that ALD Al_2O_3 can be a promising candidate for LATP protection against polysulfide species due to its thin film nature that can allow Li^+ ions to diffuse through and inherent chemical and electrochemical stability.[25–27]

Herein, we demonstrate the successful application of ALD to create an ultrathin protective coating layer on LATP for ASSLSBs with a polymer/ceramic/polymer sandwich-type (PEO/LATP/PEO) hybrid electrolyte operating at 60 °C. Compared to the pristine PEO/bare-LATP/PEO (PLP) SSE, the PEO/ALD-coated LATP/PEO (ALD-PLP) SSE presents significantly enhanced cycling performance. The results show that as few as 10 cycles of ALD of Al_2O_3 on the LATP can endow ASSLSBs with discharge capacities of 1035 mA h g^{-1} at the initial cycle and 823 mA h g^{-1} after 100 charge/discharge cycles, which is almost two times higher than that of the ASSLSB without ALD coating. The improved electrochemical performance is attributed to the protection of LATP by ALD Al_2O_3. FE-SEM studies show that bare LATP is pulverized after long-term cycling, whereas with ALD coating, the LATP stability is greatly improved. XRD and XPS studies indicate that ALD coating can effectively prevent the reduction of Ti in LATP by polysulfides. This investigation discloses a new avenue to tackle the instability problem between the SSE and electrodes for the development of all-solid-state batteries.

Experimental section

Preparation of a PEO-based solid-state electrolyte

Polyethylene oxide (PEO, MW 600 000) and $LiClO_4$ (purity, 99.9%) were carefully dried before use. 0.093 g of $LiClO_4$ was first dissolved in acetonitrile (AN) and stirred over 5 h. Then 0.6 g of PEO was added to the solution and stirred overnight. The resulting homogeneous mixture containing PEO–$LiClO_4$ was coated onto a Teflon evaporating dish and dried at 60 °C for 24 h in vacuum to obtain the PEO-based solid polymer electrolyte (SPE) membrane. The thickness of the SPE is 70 ± 10 μm.

Preparation of NASICON-type solid-state electrolyte LATP for ALD coating

NASICON-type SSE $Li_{1.4}Al_{0.4}Ti_{1.6}(PO_4)_3$ (LATP) was synthesized by a solid-state reaction method.[28] Stoichiometric amounts of Li_2CO_3, Al_2O_3, TiO_2, and $NH_4H_2PO_4$ were first mixed using a ball milling method at 300 rpm for 5 h in a zirconia vessel with zirconia balls. Then the mixed powders were calcined at 700 °C for 2 h. The obtained powders were ground with polyvinyl alcohol (PVA) as the binder before being pressed into 1.2 cm diameter pellets at 250 MPa. The as-pressed pellets were calcined at 900 °C for 6 h. The obtained LATP SSE pellets were polished using sandpaper down to a thickness of 500 ± 30 μm. The polished LATP pellets were coated with an Al_2O_3 layer by atomic layer deposition (ALD). Then one surface of this ALD coated LATP was polished again to remove the ALD coating. LATP with one ALD coated surface was assembled into all solid-state Li–S batteries with the ALD coated surface toward the sulfur cathode. Different thicknesses of ALD Al_2O_3 were directly coated on the surfaces of LATP pellets in an ALD reactor (Gemstar-8 ALD system) by controlling the ALD cycle number. Trimethylaluminum (TMA) and water (H_2O) were used as the precursors and the deposition temperature was set as 120 °C. The growth rate of ALD Al_2O_3 at 120 °C is 0.1 nm per cycle.[29,30]

Preparation of the sulfur electrode

Commercial carbon black (Ketjenblack EC-600, US) and sulfur powder (99.5%, Sigma-Aldrich) were dried at 70 °C overnight in a vacuum oven. Then carbon black and a certain amount of sulfur were mixed together and transferred to a sealed steel reactor. The reactor was heated at 150 °C for 10 h and then at 300 °C for 3 h. The obtained carbon–sulfur composites (C–S) maintained a 65 wt% sulfur loading (Fig. S1†). The electrodes were prepared by slurry casting on carbon-coated aluminum foil. The slurry mass ratio of C–S composites, acetylene black, and polyvinylidene fluoride (PVDF) is 8 : 1 : 1. The as-prepared electrodes were finally dried at 60 °C overnight in a vacuum oven. The final loading of sulfur in the cathode electrode is 0.6–1 mg cm^{-2}.

Preparation of fully reduced-LATP

Fully reduced LATP was prepared by soaking pristine LATP pellets in a polysulfide solution containing 1 M Li_2S_6 for 1 week. The reduced LATP was used for XRD and XPS study.

Electrochemical characterization

PEO-based SPE membranes were cut into a circular shape for electrochemical impedance spectroscopy (EIS) testing using stainless steel as the blocking electrode. For the EIS testing of LATP SSE pellets, a layer of gold was deposited on the surface of pellets using sputtering and used as blocking electrodes. The

stainless steel was also applied in the EIS testing of the PEO/LATP/PEO (PLP) sandwich-type hybrid electrolyte because PEO-based SPE has good contact ability with stainless steel and LATP. EIS was performed on the versatile multichannel potentiostat 3/Z (VMP3) by applying an AC voltage of 10 mV amplitude in the 500 kHz to 0.01 Hz frequency range. The EIS of the PEO-based SPE and PLP sandwich-type hybrid electrolyte were measured using stainless steel as the blocking electrode and the electrolytes were preheated to 80 °C for over 2 h before measurement.

CR-2032 type coin cells were assembled in an argon-filled glovebox. The first type of coin cells consisted of a C–S cathode, commercial liquid electrolyte (containing 1 M LiTFSI salt dissolved in dioxolane (DOL) : dimethoxyethane (DME) of a 1 : 1 volume ratio and $LiNO_3$ as an additive), and lithium metal anode. The second type of coin cells consisted of a C–S cathode, PEO-based SPE, and lithium metal anode. The third type of coin cells consisted of a C–S cathode, PLP (or ALD-LATP) sandwich-type hybrid electrolyte, and lithium metal anode. A detailed illustration of the battery configurations is presented in Fig. S2.† Cyclic voltammograms were collected on a versatile multichannel potentiostat 3/Z (VMP3) at a scan rate of 0.1 mV s^{-1} between 1.5 V and 3.0 V (*vs.* Li/Li^+) for the liquid electrolyte Li–S battery and 1.0–3.0 V for the all solid-state Li–S battery. All of the batteries were tested by holding at 60 °C after assembling for 24 h. Charge/discharge characteristics were galvanostatically tested in the range of 1.5–3.0 V for the liquid electrolyte Li–S battery and 1.0–3.0 V for the all solid-state Li–S battery at 60 °C using LAND Battery Test equipment with a current density of 0.1C.

Physical characterization

The morphologies of the samples were characterized using a Hitachi S-4800 field emission scanning electron microscope (FE-SEM) equipped with energy dispersive spectroscopy (EDS). Thermogravimetric analysis (TGA) was carried out in a nitrogen atmosphere from room temperature to 700 °C at a heating rate of 10 °C min^{-1} on a SDT Q600 (TA Instruments). Phase analysis was performed by X-ray diffraction (XRD) (Bruker D8 Advance, Cu Kα X-ray source). X-ray photoelectron spectroscopy was conducted on a Kratos AXIS Ultra Spectrometer system. High energy X-ray photoelectron spectroscopy (HEXPS) measurements at Ti 1s were performed at the Soft X-Ray Microcharacterization Beamline (SXRMB) at the Canadian Light Source (CLS) located at the University of Saskatoon, Saskatoon, Canada. The photon energy used for HEXPS is 8 keV with a probing depth of around 4 nm.

Results and discussion

SSE LATP was prepared by a solid-state reaction method,[28] and the surface modification was carried out by depositing ALD Al_2O_3 onto LATP pellets before ASSLSB assembly (Fig. 1 shows the schematic diagram of a LATP pellet, an ALD coated LATP pellet and the configurations of ASSLSBs). One of the surfaces of the LATP pellet (facing anode) was polished after the ALD process to remove the ALD coating. The phase of LATP after ALD coating was evaluated by XRD (Fig. 1b), where the results clearly indicate that there are no impurities introduced by the ALD process. On the other hand, the PEO-based SPE was prepared by a solution casting method.[31] The sandwich type polymer/ceramic/polymer SSE is assembled by stacking PEO, a LATP pellet, and another layer of PEO. The detailed configurations of the ASSLSBs are presented in Fig. 1a.

The ionic conductivities of the PEO-based SPE and PLP SSE were evaluated by electrochemical impedance spectroscopy (EIS). Temperature dependent ionic conductivities of different

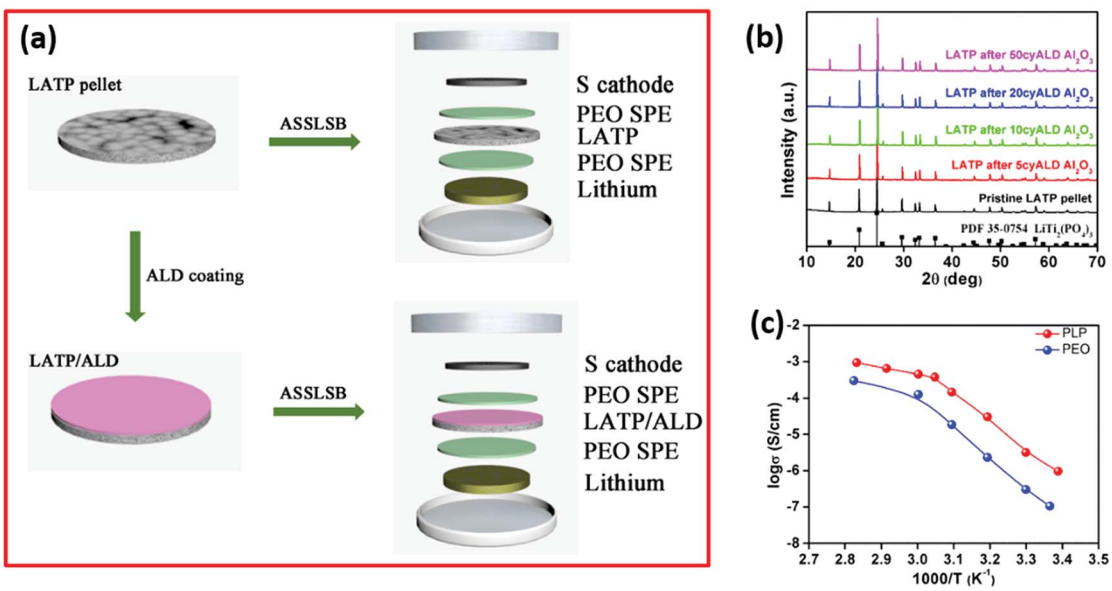

Fig. 1 (a) A schematic diagram showing the preparation of an ALD coated LATP SSE and the configuration of ASSLSBs. (b) XRD patterns of LATP with different numbers of ALD coating cycles. (c) Temperature dependent ionic conductivity of the PEO-based SPE and PLP sandwich-type hybrid electrolyte.

SSEs are illustrated in Fig. 1c. PEO-based SPE has a low ionic conductivity on the order of $\sim 10^{-8}$ S cm^{-1} at room temperature (RT), which is similar to a previously reported result.[31] At an elevated temperature of ~60 °C, the ionic conductivity increases to the order of 10^{-4} S cm^{-1}. The ionic conductivity of the PLP SSE is higher than that of the SPE, which is 4.8×10^{-4} S cm^{-1} at 60 °C, due to the existence of the LATP ceramic SSE.

Cyclic voltammetry (CV) measurements have been conducted to analyze the electrochemical reaction mechanism of the ASSLSBs with the PEO-based SPE and PLP with or without ALD modification at 60 °C. Fig. 2a–c illustrate the CV curves of Li–S batteries with the PEO-based SPE, PLP and ALD-PLP SSEs. A conventional Li–S battery with commercialized ether-based liquid electrolyte was also assembled using the same S/C cathode to make a fair comparison (Fig. S8†). For the liquid-based Li–S battery, two well defined cathodic peaks at 2.3 V and 2.1 V (*vs.* Li/Li$^+$), and one anodic peak at 2.4 V are present (Fig. S8a†). Similarly, two cathodic peaks are present at 2.4 V and 1.9 V in the ASSLSBs with PEO SPE and PLP SSEs (Fig. 2a and b), and 2.3 V and 1.7 V in the ASSLSB with the ALD-PLP SSE (Fig. 2c). The two cathodic peaks in the CV curves of the ASSLSBs indicate that the electrochemical reactions are similar to that in the liquid-based Li–S battery. During the cathodic processes, sulfur is first reduced into long chain polysulfide species such as S_8^{2-} and S_6^{2-}, followed by the stepwise reduction into short chain polysulfides (S_4^{2-}, S_2^{2-}, and S^{2-}) at relatively lower voltages.[32,33] The anodic peaks of the ASSLSB with PEO SPE show strong current and fluctuation, indicating that the polysulfide intermediates dissolve and migrate through the SPE. The dissolution and migration of the polysulfide in the PEO-based SPE had been observed using *in operando* SEM and ultraviolet-visible spectroscopy studies by K. Zaghib *et al.*[9] So, the polysulfide species can migrate through the PEO SPE layer and reach the PEO/LATP interface in the PLP, and cause the reduction of Ti^{4+} in LATP, leading to the deterioration of the cycling performance of ASSLSBs. In order to protect the SSE and improve the cycling performance, ALD-derived Al_2O_3 has been applied to enhance the stability of LATP against the reduction by polysulfide species. The insulating nature of the ALD coating leads to an increase in the overall impedance (Fig. S9a†), in agreement with the two cathodic peaks of the ALD-PLP ASSLSB shifting to lower voltages and the anodic peak shifting to higher voltages compared to the uncoated PLP. After the initial CV scan, these two cathodic peaks shift to relatively higher voltages (Fig. 2c), which is possibly due to the lithiation of ALD coating layer resulting in an enhancement of the ionic conductivity and a decrease of the overall cell impedance. The lithiation of Al_2O_3 was confirmed by XPS study and the results are presented in Fig. S11.† There is no Li 1s signal for the 50 cycle ALD coated LATP before charge/discharge cycling. This is because there is no Li element in the ALD Al_2O_3 coating layer. This is Al 2p signal is related to Al_2O_3 in the same sample. After the PLP SSE was charged/discharged for 10 cycles in the ASSLSB, XPS was performed on the ALD coated surface of the LATP, and a strong Li

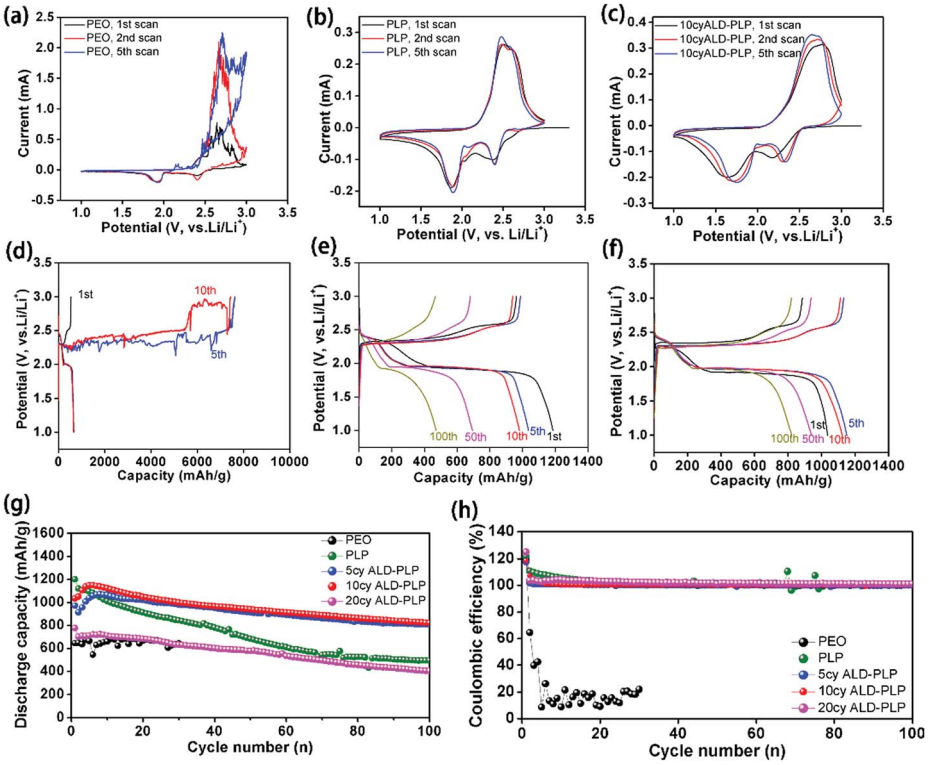

Fig. 2 Cyclic voltammetry curves of a (a) PEO SPE Li–S battery, (b) ASSLSB with a PLP sandwich electrolyte and (c) ASSLSB with 10 cycles of ALD-PLP. Charge/discharge potential profiles of ASSLSB (d) with a PEO SPE, (e) with a PLP SSE and (f) with 10 cycles of ALD-PLP SSE; (g) cycling performance of Li–S batteries with different electrolytes and its corresponding coulombic efficiency (h). All cycling was performed at a current density of 0.1C (1C = 1670 mA h g^{-1}) and 60 °C.

1s peak was observed. Also, we found a shift of the Al 2p to a lower binding energy, which confirms the lithiation of Al_2O_3 to $LiAlO_x$ after battery cycling. Similar results had been reported by X. Xiao *et al.* and Y. S. Jung *et al.*[34,35]

To evaluate the electrochemical performance and stability of Li–S batteries, galvanostatic charge/discharge testing was performed at high temperature (60 °C). The Li–S battery with a liquid-based electrolyte has two discharge plateaus, one at 2.3 V and another at 2.1 V, in addition to a charge plateau at 2.2 V (Fig. S8b†). Similar behaviours are observed in ASSLSBs with PEO, PLP and ALD-PLP SSEs where two discharge plateaus are present (Fig. 2d–f). For ASSLSBs with PLP and ALD-PLP SSEs, two charge potential plateaus are well defined, indicating clear stepwise oxidation of short chain polysulfide species. In contrast, the stepwise oxidation process is not obvious in the liquid-based Li–S battery. The reason behind this phenomenon is possibly related to the high viscosity of the SPE, which can effectively limit the diffusion rate of polysulfides compared to their fast transport in liquid electrolyte.

The long-term cycling performance of the liquid-based Li–S batteries and ASSLSBs is displayed in Fig. S8c† and 2g, respectively. The Li–S batteries were first discharged then charged, and the coulombic efficiency was calculated from the ratio of discharge capacity to charge capacity. From Fig. S8c,† it can be seen that the liquid-based Li–S battery delivers an initial discharge capacity of 1134 mA h g^{-1} which then rapidly decays to 295 mA h g^{-1} after 100 charge/discharge cycles. The coulombic efficiency of the liquid-based Li–S battery is very low during the first 30 cycles, which can be attributed to the polysulfide shuttle effect. In comparison, the ASSLSB with PEO can yield a discharge capacity around 645 mA h g^{-1} with a very low coulombic efficiency fluctuating between 0 and 30% and a severe overcharging problem is observed (Fig. 2d), which is consistent with the result reported by M. Lécuyer *et al.*[36] Similar to the liquid-based system, this poor coulombic efficiency can also be attributed to the polysulfide shuttle effect. However, the ASSLSB with the PLP SSE displays an initial discharge capacity of 1201 mA h g^{-1} with a coulombic efficiency of 122% in the first cycle. The coulombic efficiency values of over 100% indicate that some of the discharged active material is irreversibly lost. This is possibly because of the dissolution of the polysulfides in the PEO-based SPE and the reduction of the LATP consuming polysulfides. However, after 5 charge/discharge cycles, the ASSLSBs with PLP and ALD-PLP show stabilization of the coulombic efficiencies at around 100% for 100 cycles, which indicates the inhibition of polysulfide shuttling and good retention of the active material. After 100 charge/discharge cycles, the ASSLSB with the PLP SSE has a discharge capacity of 494 mA h g^{-1}, which is higher than that of the liquid-based system. However, the battery still shows dramatic capacity fade over extended cycling. The cycling performance of the lithium symmetric cell with a PLP SSE is illustrated in Fig. S12.† This shows that with an ultra-long cycling time and increased cycling numbers, there is no voltage drop or over-potential increase, which indicates that PLP is ultra-stable in lithium symmetric cells without lithium dendrite formation and reduction of LATP. However, in the ASSLSB with the PLP SSE, there are charge/discharge intermediate products, polysulfides, which are dissolvable in PEO-based SPEs and thus they can transfer to the PEO/LATP interface to react with LATP causing the reduction of LATP. With extensive cycling of the ASSLSB, the degradation of LATP is progressive. With the degradation of LATP, polarization in the charge/discharge curves of ASSLSB with PLP (as shown in Fig. 2e) increases. Therefore, the capacity fading of the ASSLB is caused by the degradation of PLP. The degradation of PLP is caused by the reduction of LATP by polysulfides. Thus, the protection of PLP from reduction is extremely important for the enhancement of ASSLSBs' performance.

Therefore, an ultra-thin Al_2O_3 was deposited on LATP by ALD to inhibit the reduction by the polysulfide. An optimization of the Al_2O_3 thickness was done and the results are presented in Fig. 2g. With 10 cycles of ALD coating, the best cycling performance could be achieved. A thicker coating layer will result in higher overall resistance (Fig. S9†) and lower the discharge capacity significantly. With 10 cycles of ALD coating, the increase of the overall resistance is not significant compared to the ASSLSB with the PLP electrolyte (Fig. S9a†). The initial discharge capacity of the ASSLSB with 10 cycles of ALD ALD-PLP SSE is 1035 mA h g^{-1}, which is comparable to that of liquid-based Li–S and PLP ASSLSBs. After several initial cycles, the discharge capacity increases to 1150.5 mA h g^{-1}. This is because the ALD Al_2O_3 coating was lithiated after several charge/discharge cycles and the resistance of the ASSLSB therefore decreases, resulting in increased capacity (as supported by the XPS results shown in Fig. S14†). From the EIS results (Fig. S9†) we can find that the impedance of the ASSLSB with ALD coating decreased after charge/discharge, which also supports this hypothesis. A similar phenomenon had been reported in Al_2O_3 coated $LiCoO_2$ batteries.[35] After 100 charge/discharge cycles, the ALD-PLP ASSLSB can still deliver a capacity of 823 mA h g^{-1}, which is almost twice of liquid-based and PLP-based Li–S batteries. This result is much better than the previous reported all-solid-state Li–S battery performances. (Table S1†).

To investigate the decomposition of the SSE by the polysulfide and to study the effect of ALD coating on the protection of LATP in ASSLSBs, cross-sectional SEM of LATP facing the sulfur cathode is conducted. Fig. 3a illustrates the cross-sectional image of the pristine LATP after sintering and polishing. The LATP pellet presents a flat surface and has a grain size of approximately 5 μm with good intergranular contact. However, after 100 charge/discharge cycles, the LATP interface on the sulfur cathode side shows grain pulverization and structural collapse (Fig. 3b). The pulverized LATP particles range in size of 100–500 nm (Fig. S13†). Furthermore, the pulverization can be observed to occur as deep as 50 μm into the LATP pellet (Fig. 3b). The destruction of the LATP structure indicates severe reduction of LATP by polysulfide species, which is the reason for the rapid capacity fading. By applying 5 cycles of ALD, the deterioration of the interface can be effectively inhibited. As a matter of fact, the formation of small secondary particles is rarely observed and the surface of the ALD-protected LATP is much flatter (Fig. 3c) compared to that of the bare LATP after cycling. With a thicker ALD coating, the formation of secondary particles is almost completely inhibited and the cycled LATP can retain a uniform grain size similar to the pristine sample (Fig. 3d–f). The crystal phase structure of LATP

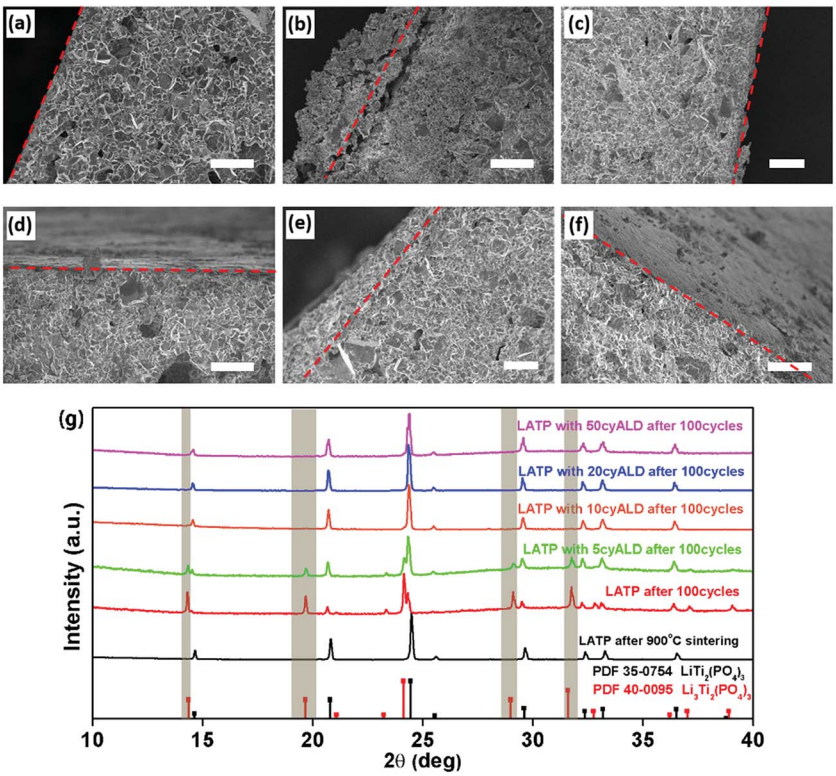

Fig. 3 Cross sectional SEM images of (a) pristine LATP, (b) bare LATP after 100 charge/discharge cycles, (c) 5 cycles of ALD coated LATP after 100 charge/discharge cycles, (d) 10 cycles of ALD coated LATP after 100 charge/discharge cycles, (e) 20 cycles of ALD coated LATP after 100 charge/discharge cycles, and (f) 50 cycles of ALD coated LATP after 100 charge/discharge cycles. The red dotted lines indicate the cross section of the LATP side at the cathode interface. Scale bar: 20 μm. (g) Comparison of the XRD patterns of LATP after sintering and LATP with different cycle numbers of ALD coating after 100 charge/discharge cycles in ASSLSBs. The XRD peaks corresponding to the reduced LATP phase are highlighted.

facing the sulfur cathode side after cycling was characterized by XRD (Fig. 3g). Pristine LATP after sintering exhibits a pure $LiTi_2(PO_4)_3$ phase where Ti exists as Ti^{4+}. In contrast, the LATP after 100 cycles shows strong peaks related to the $Li_3Ti_2(PO_4)_3$ phase, in which Ti is reduced to Ti^{3+}. Upon protecting the interface with ALD, the intensities of the peaks associated with the $Li_3Ti_2(PO_4)_3$ phase decrease with the use of 5 ALD cycles, and further disappears with thicker coatings of 10, 20, and 50 ALD cycles. The prevention of Ti reduction indicates the excellent protection effect of the ALD Al_2O_3 coating.

To study the chemical states of Ti in LATP before and after cycling, synchrotron-based high energy X-ray photoelectron spectroscopy (HEXPS) was utilized to study the LATP interface. The Ti 1s XPS of pristine LATP is shown in Fig. S14a,† where a single peak at 4970 eV is presented. This peak can be indexed to Ti^{4+} of the $LiTi_2(PO_4)_3$ phase in the pristine LATP. After complete reduction by polysulfides, the Ti 1s spectrum shows a decrease in binding energy to 4969 eV (Fig. S14b†), which is indexed as reduced-Ti. To calculate the content of Ti^{4+} and reduced-Ti in the LATP SSE after 100 charge/discharge cycles in ASSLSBs, XPS peaks of 4970 and 4969 eV were used to fit the spectrum and the results are presented in Fig. 4a–d and Table S2.† Bare LATP after cycling has a strong Ti 1s peak related to the reduced-Ti and a weak peak corresponding to Ti^{4+}, which indicates significant reduction of LATP by polysulfides. With the presence of ALD protection, the peak associated with reduced-Ti species decreased significantly. The contents of Ti^{4+} and reduced-Ti for bare LATP after 100 charge/discharge cycles are 28.7% and 71.3%, respectively. With ALD coating, the content of reduced-Ti decreases to 43.2% for 5 cycles of ALD-LATP, 37.4% for 10 cycles ALD-LATP and 29.2% for 20 cycles of ALD-LATP. Table S2† summarizes the fitting results of the XPS spectra. Clearly, a thicker ALD coating is more effective in preventing the reduction of LATP by polysulfide species.

To summarize the aforementioned results with respect to their cell configurations, the schematic diagrams of the tested ASSLSB systems and the role of the ALD Al_2O_3 coating are illustrated in Fig. 5. In the ASSLSB with the PLP SSE, a serious reduction of LATP by polysulfides happens and a very thick layer of reduced-LATP (r-LATP) is formed on the surface of LATP (toward the sulfur cathode side) accompanied by degradation of structural features after being charged/discharged for 100 cycles (Fig. 5a and d (bottom)). However, with 10 cycles of ALD coating, the reduction of LATP is significantly reduced and a very thin layer of r-LATP is formed on the LATP surface (Fig. 5b and e (bottom)). Thus, with ALD protection, LATP can maintain its electrochemical properties and endow the ASSLSB with stable, long cycle performance.

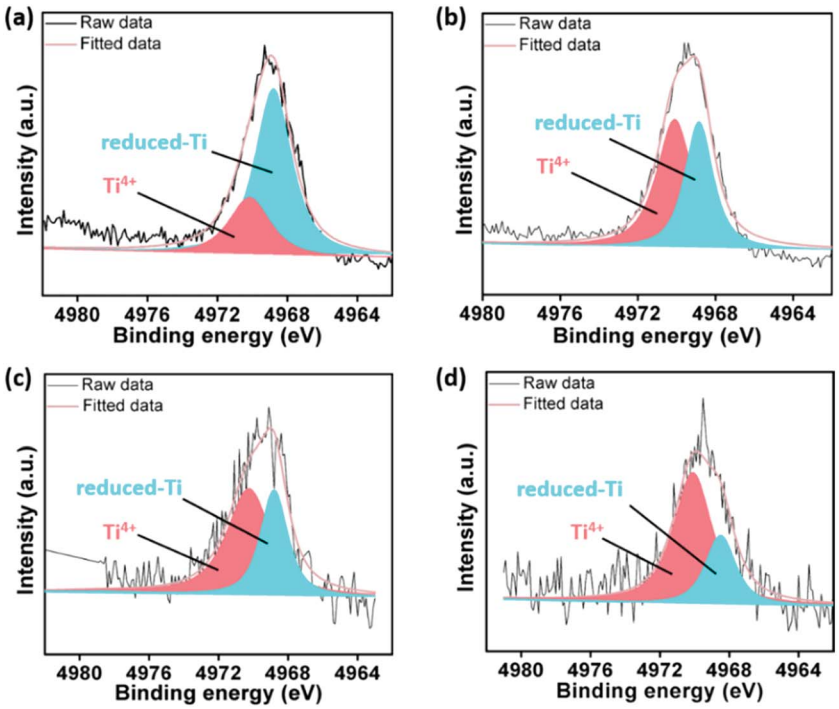

Fig. 4 Ti 1s XPS of (a) bare LATP, (b) 5 cycles ALD-LATP, (c) 10 cycles of ALD-LATP and (d) 20 cycles of ALD-LATP after 100 charge/discharge cycles in ASSLSBs. All XPS studies were conducted on the LATP surface facing the sulfur cathode.

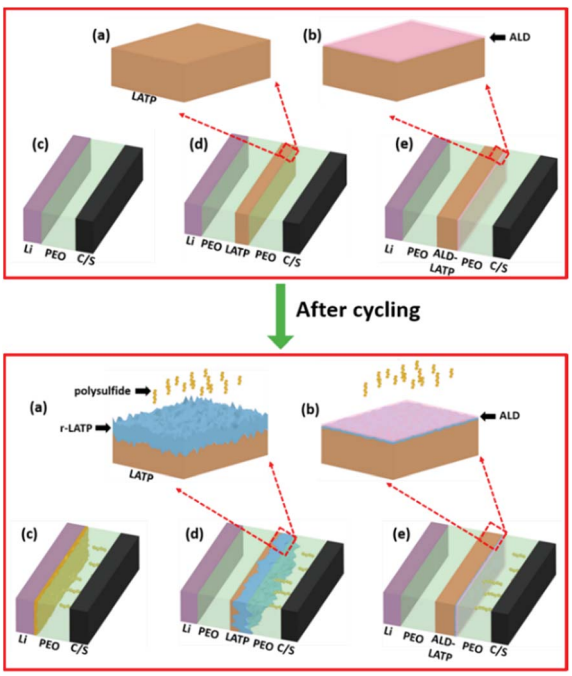

Fig. 5 Magnified schematic diagram showing (a) bare LATP (top) and the reduction of LATP upon cycling (bottom), and (b) protection of the bulk LATP by ALD before (top) and after (bottom) cycling. The cell configurations of (c) Li/PEO/S ASSLSB, (d) Li/PLP/S ASSLSB, and (e) Li/ALD-PLP/S ASSLSB.

Conclusions

In conclusion, we report an innovative and effective strategy to enhance the cycling stability of ASSLSBs *via* solving the instability between the SSE and polysulfide species. By preventing the reduction of polysulfides toward LATP during battery operation using ALD surface engineering on the LATP SSE, the rapid capacity fading of the ASSLSB can be avoided. Using ALD-derived Al_2O_3-coated LATP, the reduction of LATP by polysulfide species can be effectively eliminated and the electrochemical performance of ASSLSBs can be significantly enhanced. As a result, the ASSLSB with ALD-PLP shows a stable cycling performance with a discharge capacity of 823 mA h g^{-1} after 100 charge/discharge cycles, which is two times higher than that of the unprotected SSE and Li–S battery with a liquid-based electrolyte. This work sheds light on addressing the major challenge of the instability problem between the LATP SSE and sulfur cathode, paving the way to develop a high energy density ASSLSB.

Statement of contributions

J. Liang, Q. Sun and X. Sun conceived the idea and experiments; J. Liang carried out the synthesis and performed the materials characterization and electrochemical performance testing. Zhao and Y. Sun helped to conduct ALD coating experiments. C. Wang and Y. Liu helped with LATP solid-state electrolyte preparations; W. Li, M. Li and D. Wang assisted in the Synchrotron XPS measurements; X. Li, K. Adair, R. Li, L. Zhang, R. Yang, S. Lu and H. Huang participated in data analysis and

discussion; X. Sun supervised the overall project. All authors discussed the results and commented on the manuscript.

Conflicts of interest

There are no conflicts to declare.

Acknowledgements

This work was supported by the China Automotive Battery Research Institute-Western University Joint Laboratory, Natural Sciences and Engineering Research Council of Canada (NSERC), Canada Research Chair (CRC) Program, Ontario Research Fund, Canada Light Source (CLS), University of Western Ontario, and China Scholarship Council (CSC).

Notes and references

1 X. Liang, C. Hart, Q. Pang, A. Garsuch, T. Weiss and L. F. Nazar, *Nat. Commun.*, 2015, **6**, 5682.
2 Y. Yang, G. Zheng and Y. Cui, *Chem. Soc. Rev.*, 2013, **42**, 3018–3032.
3 X. Tao, Y. Liu, W. Liu, G. Zhou, J. Zhao, D. Lin, C. Zu, O. Sheng, W. Zhang, H.-W. Lee and Y. Cui, *Nano Lett.*, 2017, **17**, 2967–2972.
4 H. J. Peng, J. Q. Huang, X. B. Cheng and Q. Zhang, *Adv. Energy Mater.*, 2017, **7**, 1700260.
5 S. Xiong, M. Regula, D. Wang and J. Song, *Electrochemical Energy Reviews*, 2018, **1**, 388–402.
6 Y. V. Mikhaylik and J. R. Akridge, *J. Electrochem. Soc.*, 2004, **151**, A1969–A1976.
7 J. Yue, M. Yan, Y. X. Yin and Y. G. Guo, *Adv. Funct. Mater.*, 2018, 1707533.
8 Y.-Z. Sun, J.-Q. Huang, C.-Z. Zhao and Q. Zhang, *Sci. China Chem.*, 2017, **60**, 1508–1526.
9 H. Marceau, C.-S. Kim, A. Paolella, S. Ladouceur, M. Lagacé, M. Chaker, A. Vijh, A. Guerfi, C. M. Julien, A. Mauger, M. Armand, P. Hovington and K. Zaghib, *J. Power Sources*, 2016, **319**, 247–254.
10 B. H. Jeon, J. H. Yeon, K. M. Kim and I. J. Chung, *J. Power Sources*, 2002, **109**, 89–97.
11 K. K. Fu, Y. Gong, G. T. Hitz, D. W. McOwen, Y. Li, S. Xu, Y. Wen, L. Zhang, C. Wang and G. Pastel, *Energy Environ. Sci.*, 2017, **10**, 1568–1575.
12 Z. Lin, Z. Liu, N. J. Dudney and C. Liang, *ACS Nano*, 2013, **7**, 2829–2833.
13 R.-c. Xu, X.-h. Xia, S.-h. Li, S.-z. Zhang, X.-l. Wang and J.-p. Tu, *J. Mater. Chem. A*, 2017, **5**, 6310–6317.
14 F. Han, J. Yue, X. Fan, T. Gao, C. Luo, Z. Ma, L. Suo and C. Wang, *Nano Lett.*, 2016, **16**, 4521–4527.
15 Q. Wang, Z. Wen, J. Jin, J. Guo, X. Huang, J. Yang and C. Chen, *Chem. Commun.*, 2016, **52**, 1637–1640.
16 W. Zhou, S. Wang, Y. Li, S. Xin, A. Manthiram and J. B. Goodenough, *J. Am. Chem. Soc.*, 2016, **138**, 9385–9388.
17 B. Liu, Y. Gong, K. Fu, X. Han, Y. Yao, G. Pastel, C. Yang, H. Xie, E. D. Wachsman and L. Hu, *ACS Appl. Mater. Interfaces*, 2017, **9**, 18809–18815.
18 P. R. Chinnam and S. L. Wunder, *ACS Energy Lett.*, 2016, **2**, 134–138.
19 R. Chen, W. Qu, X. Guo, L. Li and F. Wu, *Mater. Horiz.*, 2016, **3**, 487–516.
20 S. Wang, Y. Ding, G. Zhou, G. Yu and A. Manthiram, *ACS Energy Lett.*, 2016, **1**, 1080–1085.
21 L. Wang, Y. Wang and Y. Xia, *Energy Environ. Sci.*, 2015, **8**, 1551–1558.
22 X. Meng, X. Q. Yang and X. Sun, *Adv. Mater.*, 2012, **24**, 3589–3615.
23 J. Liu and X. Sun, *Nanotechnology*, 2014, **26**, 024001.
24 Y. Zhao and X. Sun, *ACS Energy Lett.*, 2018, **3**, 899–914.
25 D. Wang, J. Yang, J. Liu, X. Li, R. Li, M. Cai, T.-K. Sham and X. Sun, *J. Mater. Chem. A*, 2014, **2**, 2306–2312.
26 X. Li, J. Liu, M. N. Banis, A. Lushington, R. Li, M. Cai and X. Sun, *Energy Environ. Sci.*, 2014, **7**, 768–778.
27 X. Li, J. Liu, X. Meng, Y. Tang, M. N. Banis, J. Yang, Y. Hu, R. Li, M. Cai and X. Sun, *J. Power Sources*, 2014, **247**, 57–69.
28 C. Wang, Q. Sun, Y. Liu, Y. Zhao, X. Li, X. Lin, M. N. Banis, M. Li, W. Li, K. R. Adair, D. Wang, J. Liang, R. Li, L. Zhang, R. Yang, S. Lu and X. Sun, *Nano Energy*, 2018, **48**, 35–43.
29 J. Ferguson, A. Weimer and S. George, *Chem. Mater.*, 2004, **16**, 5602–5609.
30 M. Groner, F. Fabreguette, J. Elam and S. George, *Chem. Mater.*, 2004, **16**, 639–645.
31 F. Croce, G. Appetecchi, L. Persi and B. Scrosati, *Nature*, 1998, **394**, 456.
32 X. Li, X. Li, M. N. Banis, B. Wang, A. Lushington, X. Cui, R. Li, T.-K. Sham and X. Sun, *J. Mater. Chem. A*, 2014, **2**, 12866–12872.
33 D. Zheng, D. Liu, J. B. Harris, T. Ding, J. Si, S. Andrew, D. Qu, X.-Q. Yang and D. Qu, *ACS Appl. Mater. Interfaces*, 2016, **9**, 4326–4332.
34 X. Xiao, P. Lu and D. Ahn, *Adv. Mater.*, 2011, **23**, 3911–3915.
35 Y. S. Jung, P. Lu, A. S. Cavanagh, C. Ban, G. H. Kim, S. H. Lee, S. M. George, S. J. Harris and A. C. Dillon, *Adv. Energy Mater.*, 2013, **3**, 213–219.
36 M. Lécuyer, J. Gaubicher, M. Deschamps, B. Lestriez, T. Brousse and D. Guyomard, *J. Power Sources*, 2013, **241**, 249–254.